

Jorge Segovia

$\gamma_{\mathbf{v}}\mathbf{NN}^*$ Electrocouplings in Dyson-Schwinger Equations

Received: / Accepted:

Abstract A symmetry preserving framework for the study of continuum Quantum Chromodynamics (QCD) is obtained from a truncated solution of the QCD equations of motion or QCD's Dyson-Schwinger equations (DSEs). A nonperturbative solution of the DSEs enables the study of, e.g., hadrons as composites of dressed-quarks and dressed-gluons, the phenomena of confinement and dynamical chiral symmetry breaking (DCSB), and therefrom an articulation of any connection between them. It is within this context that we present a unified study of Nucleon, Delta and Roper elastic and transition electromagnetic form factors, and compare predictions made using a framework built upon a Faddeev equation kernel and interaction vertices that possess QCD-like momentum dependence with results obtained using a symmetry-preserving treatment of a vector \otimes vector contact-interaction. The comparison emphasises that experiment is sensitive to the momentum dependence of the running coupling and masses in QCD and highlights that the key to describing hadron properties is a veracious expression of dynamical chiral symmetry breaking in the bound-state problem.

Keywords Dyson-Schwinger equations · elastic and transition electromagnetic form factors · nucleon resonances

1 Introduction

Nonperturbative QCD poses significant challenges. Primary amongst them is a need to chart the behaviour of QCD's running coupling and masses into the domain of infrared momenta. Contemporary theory is incapable of solving this problem alone but a collaboration with experiment holds a promise for progress. This effort can benefit substantially by exposing the structure of nucleon excited states and measuring the associated transition form factors at large momentum transfer [1]. Large momenta are needed in order to pierce the meson-cloud that, often to a significant extent, screens the dressed-quark core of all baryons [2; 3]; and it is via the Q^2 evolution of form factors that one gains access to the running of QCD's coupling and masses from the infrared into the ultraviolet [4; 5].

It is within the context just described that we have performed a simultaneous treatment of elastic and transition form factors involving the Nucleon, Delta and Roper baryons in Refs. [9; 10; 11; 12; 13]. In order to address the issue of charting the behaviour of the running coupling and masses in the strong interaction sector of the Standard Model, we use a widely-accepted leading-order (rainbow-ladder) truncation of QCD's Dyson-Schwinger equations [14; 15; 16] and compare results between a QCD-based framework and a confining, symmetry-preserving treatment of a vector \otimes vector contact interaction.

Jorge Segovia
Physik-Department, Technische Universität München,
James-Franck-Str. 1, 85748 Garching, Germany
Tel.: +49-89-289-12329
Fax: +49-89-289-12325
E-mail: jorge.segovia@tum.de

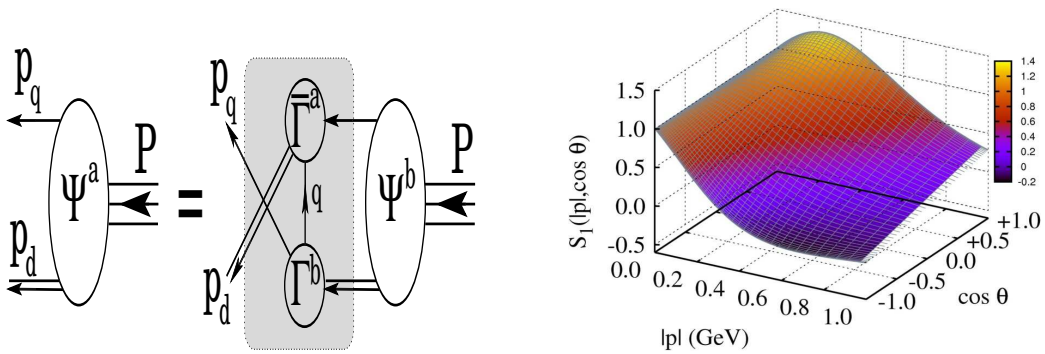


Fig. 1 *Left panel:* Poincaré covariant Faddeev equation. Ψ is the Faddeev amplitude for a baryon of total momentum $P = p_q + p_d$, where $p_{q,d}$ are, respectively, the momenta of the quark and diquark within the bound-state. The shaded area demarcates the Faddeev equation kernel: *single line*, dressed-quark propagator; Γ , diquark correlation amplitude; and *double line*, diquark propagator. *Right panel:* Dominant piece in the nucleon’s eight-component Poincaré-covariant Faddeev amplitude: $S_1(|p|, \cos \theta)$. In the nucleon rest frame, this term describes that piece of the quark–scalar–diquark relative momentum correlation which possesses zero intrinsic quark–diquark orbital angular momentum, i.e. $L = 0$ before the propagator lines are reattached to form the Faddeev wave function. Referring to Fig. 1, $p = P/3 - p_q$ and $\cos \theta = p \cdot P / \sqrt{p^2 P^2}$. The amplitude is normalised such that its U_0 Chebyshev moment is unity at $|p| = 0$.

A unified QCD-based description of elastic and transition form factors involving the nucleon and its resonances has acquired additional significance owing to substantial progress in the extraction of transition electrocouplings, g_{vNN^*} , from meson electroproduction data, obtained primarily with the CLAS detector at the Thomas Jefferson National Accelerator Facility (JLab). The electrocouplings of all low-lying N^* states with mass less-than 1.6 GeV have been determined via independent analyses of π^+n , π^0p and $\pi^+\pi^-p$ exclusive channels [6; 7]; and preliminary results for the g_{vNN^*} electrocouplings of most high-lying N^* states with masses below 1.8 GeV have also been obtained from CLAS meson electroproduction data [1; 8].

2 Baryon structure

Dynamical chiral symmetry breaking (DCSB) is a theoretically-established feature of QCD and the most important mass generating mechanism for visible matter in the Universe, being responsible for approximately 98% of the proton’s mass. A fundamental expression of DCSB is the behaviour of the quark mass-function, $M(p)$, which is a basic element in the dressed-quark propagator:

$$S(p) = 1/[i\gamma \cdot p A(p^2) + B(p^2)] = Z(p^2)/[i\gamma \cdot p + M(p^2)], \quad (1)$$

and may be obtained as a solution to QCD’s most basic fermion gap equation, i.e. the Dyson-Schwinger equation (DSE) for the dressed-quark propagator [16]. The nontrivial character of the mass function arises primarily because a dense cloud of gluons comes to clothe a low-momentum quark. It explains how an almost-massless parton-like quark at high energies transforms, at low energies, into a constituent-like quark with an effective mass of around 350 MeV.

DCSB ensures the existence of nearly-massless pseudo-Goldstone modes (pions). Another equally important consequence of DCSB is less well known. Namely, any interaction capable of creating pseudo-Goldstone modes as bound-states of a light dressed-quark and -antiquark, and reproducing the measured value of their leptonic decay constants, will necessarily also generate strong colour-antitriplet correlations between any two dressed quarks contained within a baryon. Although a rigorous proof within QCD cannot be claimed, this assertion is based upon an accumulated body of evidence, gathered in two decades of studying two- and three-body bound-state problems in hadron physics. No realistic counter examples are known; and the existence of such diquark correlations is also supported by simulations of lattice QCD.

The existence of diquark correlations considerably simplifies analyses of the three valence-quark scattering problem and hence baryon bound states because it reduces that task to solving a Poincaré covariant Faddeev equation depicted in the left panel of Fig. 1. Two main contributions appear in the binding energy: i) the formation of tight diquark correlations and ii) the quark exchange depicted in

the shaded area of the left panel of Fig. 1¹. This exchange ensures that diquark correlations within the baryon are fully dynamical: no quark holds a special place because each one participates in all diquarks to the fullest extent allowed by its quantum numbers. Attending to the quantum numbers of the nucleon and Roper, scalar-isoscalar and pseudovector-isotriplet diquark correlations are dominant. For the Δ -baryon, only the pseudovector-isotriplet ones are present.

The quark+diquark structure of the nucleon is elucidated in the right panel of Fig. 1, which depicts the leading component of its Faddeev amplitude: with the notation of Ref. [11], $S_1(|p|, \cos\theta)$, computed using the Faddeev kernel described therein. This function describes a piece of the quark+scalar-diquark relative momentum correlation. Notably, in this solution of a realistic Faddeev equation there is strong variation with respect to both arguments. Support is concentrated in the forward direction, $\cos\theta > 0$, so that alignment of p and P is favoured; and the amplitude peaks at $(|p| \simeq M_N/6, \cos\theta = 1)$, whereat $p_q \sim p_d \sim P/2$ and hence the natural relative momentum is zero. In the antiparallel direction, $\cos\theta < 0$, support is concentrated at $|p| = 0$, i.e. $p_q \sim P/3, p_d \sim 2P/3$.

3 The $\gamma^*N \rightarrow Nucleon$ Transition

The strong diquark correlations must be evident in many physical observables. We focus our attention on the flavour separated versions of the Dirac and Pauli form factors of the nucleon. The upper panels of Figure 2 display the proton's flavour separated Dirac and Pauli form factors. The salient features of the data are: the d -quark contribution to F_1^p is far smaller than the u -quark contribution; $F_2^d/\kappa_d > F_2^u/\kappa_u$ on $x < 2$ but this ordering is reversed on $x > 2$; and in both cases the d -quark contribution falls dramatically on $x > 3$ whereas the u -quark contribution remains roughly constant. Our calculations are in semi-quantitative agreement with the empirical data.

It is natural to seek an explanation for the pattern of behaviour in the upper panels of Fig. 2. We have mentioned that the proton contains scalar and pseudovector diquark correlations. The dominant piece of its Faddeev wave function is $u[ud]$; namely, a u -quark in tandem with a $[ud]$ scalar correlation, which produces 62% of the proton's normalisation. If this were the sole component, then photon- d -quark interactions within the proton would receive a $1/x$ suppression on $x > 1$, because the d -quark is sequestered in a soft correlation, whereas a spectator u -quark is always available to participate in a hard interaction. At large $x = Q^2/M_N^2$, therefore, scalar diquark dominance leads one to expect $F^d \sim F^u/x$. Available data are consistent with this prediction but measurements at $x > 4$ are necessary for confirmation.

Consider now the ratio of proton electric and magnetic form factors, $R_{EM}(Q^2) = \mu_p G_E(Q^2)/G_M(Q^2)$, $\mu_p = G_M(0)$. A clear conclusion from lower-left panel of Fig. 2 is that pseudovector diquark correlations have little influence on the momentum dependence of $R_{EM}(Q^2)$. Their contribution is indicated by the dotted (blue) curve, which was obtained by setting the scalar diquark component of the proton's Faddeev amplitude to zero and renormalising the result to unity at $Q^2 = 0$. As apparent from the dot-dashed (red) curve, the evolution of $R_{EM}(Q^2)$ with Q^2 is primarily determined by the proton's scalar diquark component. As we have explained above, in this component, the valence d -quark is sequestered inside the soft scalar diquark correlation so that the only objects within the nucleon which can participate in a hard scattering event are the valence u -quarks. The scattering from the proton's valence u -quarks is responsible for the momentum dependence of $R_{EM}(Q^2)$. However, the dashed (green) curve in the lower-left panel of Fig. 2 reveals something more, i.e. components of the nucleon associated with quark-diquark orbital angular momentum $L \geq 1$ in the nucleon rest frame are critical in explaining the data. Notably, the presence of such components is an inescapable consequence of the self-consistent solution of a realistic Poincaré-covariant Faddeev equation for the nucleon.

It is natural now to consider the proton ratio: $R_{21}(x) = xF_2(x)/F_1(x)$, $x = Q^2/M_N^2$, drawn in the lower-right panel of Fig. 2. As with R_{EM} , the momentum dependence of $R_{21}(x)$ is principally determined by the scalar diquark component of the proton. Moreover, the rest-frame $L \geq 1$ terms are again seen to be critical in explaining the data: the behaviour of the dashed (green) curve highlights the impact of omitting these components.

¹ Whilst an explicit three-body term might affect fine details of baryon structure, the dominant effect of non-Abelian multi-gluon vertices is expressed in the formation of diquark correlations [18].

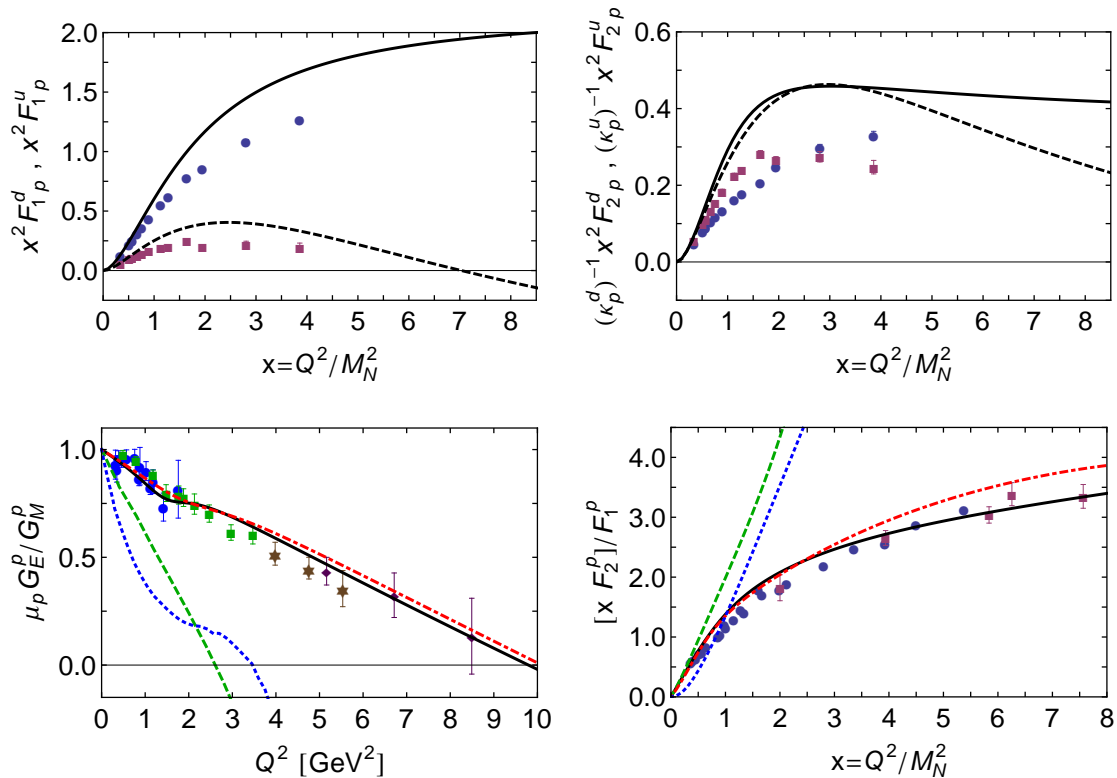


Fig. 2 *Upper-Left panel:* Computed ratio of proton electric and magnetic form factors. Curves: solid (black) – full result, determined from the complete proton Faddeev wave function and current; dot-dashed (red) – momentum-dependence of scalar-diquark contribution; dashed (green) – momentum-dependence produced by that piece of the scalar diquark contribution to the proton’s Faddeev wave function which is purely S -wave in the rest-frame; dotted (blue) – momentum-dependence of pseudovector diquark contribution. All partial contributions have been renormalised to produce unity at $Q^2 = 0$. Data: circles (blue) [19]; squares (green) [20]; asterisks (brown) [21]; and diamonds (purple) [22]. *Upper-Right panel:* Proton ratio $R_{21}(x) = xF_2(x)/F_1(x)$, $x = Q^2/M_N^2$. The legend for the curves is the same than that of the Upper-Left panel. Experimental data taken from Ref. [23]. *Lower-Left panel:* Flavour separation of the proton’s Dirac form factor as a function of $x = Q^2/M_N^2$. The results have been obtained using a framework built upon a Faddeev equation kernel and interaction vertices that possess QCD-like momentum dependence. The solid-curve is the u -quark contribution, and the dashed-curve is the d -quark contribution. Experimental data taken from Ref. [23] and references therein: circles – u -quark; and squares – d -quark. *Lower-Right panel:* Same for Pauli form factor.

4 The $\gamma^* N \rightarrow \Delta$ Transition

The electromagnetic $\gamma^* N \rightarrow \Delta$ transition is described by three Poincaré-invariant form factors [24]: magnetic-dipole, G_M^* , electric quadrupole, G_E^* , and Coulomb (longitudinal) quadrupole, G_C^* ; that can be extracted in the Dyson-Schwinger approach by a sensible set of projection operators [25]. The following ratios

$$R_{EM} = -\frac{G_E^*}{G_M^*}, \quad R_{SM} = -\frac{|\mathbf{Q}|}{2m_\Delta} \frac{G_C^*}{G_M^*}, \quad (2)$$

are often considered because they can be read as measures of the deformation of the hadrons involved in the reaction and how such deformation influences the structure of the transition current.

In considering the behaviour of the $\gamma^* N \rightarrow \Delta$ transition form factors, it is useful to begin by recapitulating upon a few facts. Note then that in analyses of baryon electromagnetic properties, using a quark model framework which implements a current that transforms according to the adjoint representation of spin-flavour $SU(6)$, one finds simple relations between magnetic-transition matrix elements [26; 27]:

$$\langle p|\mu|\Delta^+ \rangle = -\langle n|\mu|\Delta^0 \rangle, \quad \langle p|\mu|\Delta^+ \rangle = -\sqrt{2}\langle n|\mu|n \rangle; \quad (3)$$

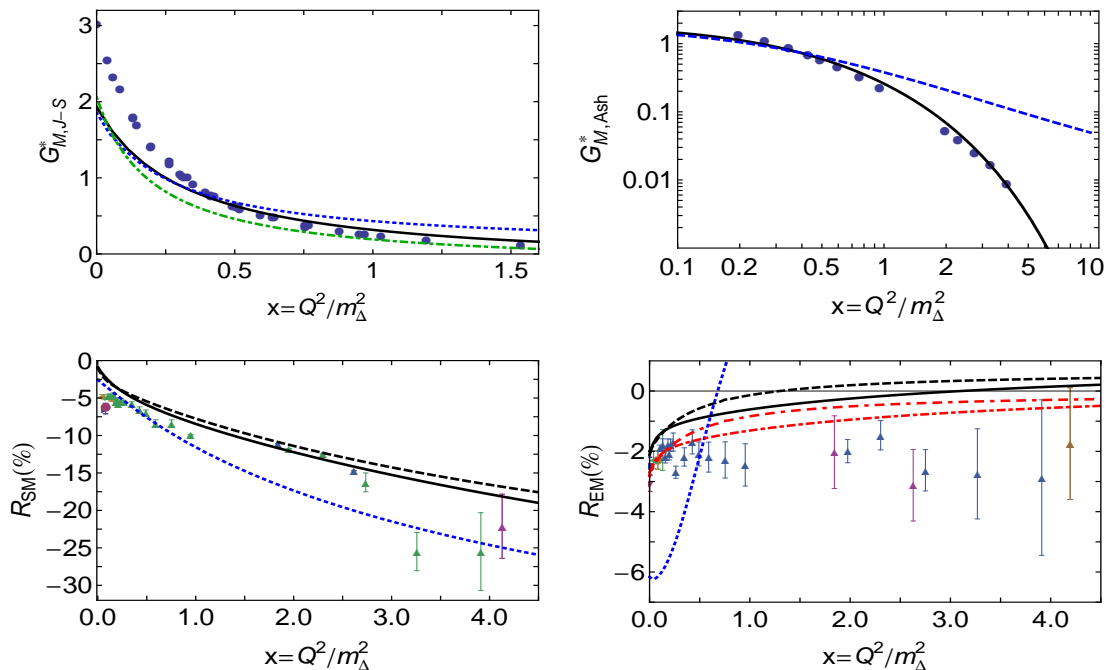


Fig. 3 *Upper-left panel* – $G_{M,J-S}^*$ result obtained with QCD-based interaction (solid, black) and with contact-interaction (CI) (dotted, blue); The green dot-dashed curve is the dressed-quark core contribution inferred using SL-model [31]. *Upper-right panel* – $G_{M,Ash}^*$ result obtained with QCD-based interaction (solid, black) and with CI (dotted, blue). *Lower-left panel* – R_{SM} prediction of QCD-based kernel including dressed-quark anomalous magnetic moment (DqAMM) (black, solid), nonincluding DqAMM (black, dashed), and CI result (dotted, blue). *Lower-right panel* – R_{EM} prediction obtained with QCD-kindred framework (solid, black); same input but without DqAMM (dashed, black); these results renormalised (by a factor of 1.34) to agree with experiment at $x = 0$ (dot-dashed, red - zero at $x \approx 14$; and dot-dash-dashed, red, zero at $x \approx 6$); and CI result (dotted, blue). The data in the panels are from references that can be found in [11].

i.e., the magnetic components of the $\gamma^*p \rightarrow \Delta^+$ and $\gamma^*n \rightarrow \Delta^0$ are equal in magnitude and, moreover, simply proportional to the neutron's magnetic form factor. Furthermore, both the nucleon and Δ are S -wave states (neither is deformed) and hence $G_E^* \equiv 0 \equiv G_C^*$.

The second entry in Eq. (3) is consistent with perturbative QCD (pQCD) [28] in the following sense: both suggest that $G_M^*(Q^2)$ should decay with Q^2 at the same rate as the neutron's magnetic form factor, which is dipole-like in QCD. It is often suggested that this is not the case empirically [29; 34]. However, as argued elsewhere [9; 10], such claims arise from a confusion between the form factors defined in the Ash [30] and Jones-Scadron [24] conventions. In addition, helicity conservation arguments within the context of pQCD enable one to make [28] the follow predictions for the ratios in Eq. (4):

$$R_{EM} \stackrel{Q^2 \rightarrow \infty}{=} 1, \quad R_{SM} \stackrel{Q^2 \rightarrow \infty}{=} \text{constant}. \quad (4)$$

These predictions are in marked disagreement with the outcomes produced by $SU(6)$ -based quark models: $R_{EM} \equiv 0 \equiv R_{SM}$. More importantly, they are inconsistent with available data [29; 34].

The upper-left panel of Fig. 3 displays the magnetic transition form factor in the Jones-Scadron convention. Our prediction obtained with a QCD-based kernel agrees with the data on $x \gtrsim 0.4$, and a similar conclusion can be inferred from the contact interaction result. On the other hand, both curves disagree markedly with the data at infrared momenta. This is explained by the similarity between these predictions and the bare result determined using the Sato-Lee (SL) dynamical meson-exchange model [31]. The SL result supports a view that the discrepancy owes to omission of meson-cloud effects in the DSEs' computations. An exploratory study of the effect of pion-cloud contributions to the mass of the nucleon and the Δ -baryon has been performed within a DSEs' framework in Ref. [32].

Presentations of the experimental data associated with the magnetic transition form factor typically use the Ash convention. This comparison is depicted in the upper-right panel of Fig. 3. One can see

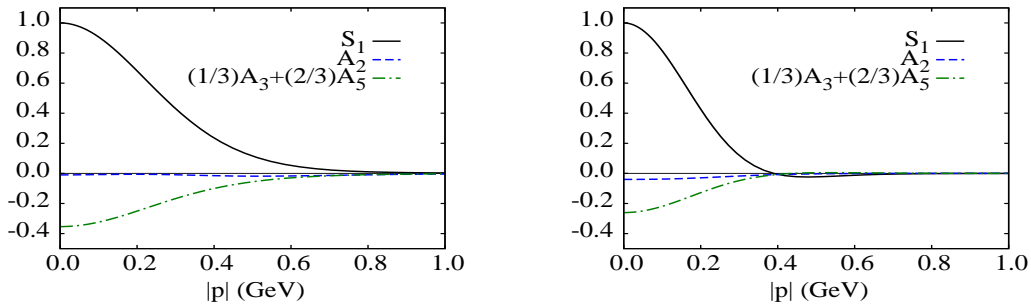


Fig. 4 *Left panel.* Zeroth Chebyshev moment of all S -wave components in the nucleon's Faddeev wave function. *Right panel.* Kindred functions for the first excited state. Legend: S_1 is associated with the baryon's scalar diquark; the other two curves are associated with the axial-vector diquark; and the normalisation is chosen such that $S_1(0) = 1$.

that the difference between form factors obtained with the QCD-kindred and CI frameworks increases with the transfer momentum. Moreover, the normalized QCD-kindred curve is in fair agreement with the data, indicating that the Ash form factor falls unexpectedly rapidly mainly for two reasons. First: meson-cloud effects provide up-to 35% of the form factor for $x \lesssim 2$; these contributions are very soft; and hence they disappear quickly. Second: the additional kinematic factor $\sim 1/\sqrt{Q^2}$ that appears between Ash and Jones-Scadron conventions and provides material damping for $x \gtrsim 2$.

Our predictions for the ratios in Eq. (2) are depicted in the lower panels of Fig. 3. The lower-left panel displays the Coulomb quadrupole ratio. Both the prediction obtained with QCD-like propagators and vertices and the contact-interaction result are broadly consistent with available data. This shows that even a contact-interaction can produce correlations between dressed-quarks within Faddeev wave-functions and related features in the current that are comparable in size with those observed empirically. Moreover, suppressing the dressed-quark anomalous magnetic moment (DqAMM) in the transition current has little impact. These remarks highlight that R_{SM} is not particularly sensitive to details of the Faddeev kernel and transition current.

This is certainly not the case with R_{EM} . The differences between the curves displayed in the lower-right panel in Fig. 3 show that this ratio is a particularly sensitive measure of diquark and orbital angular momentum correlations. The contact-interaction result is inconsistent with data, possessing a zero that appears at a rather small value of x . On the other hand, predictions obtained with QCD-like propagators and vertices can be viable. We have presented four variants, which differ primarily in the location of the zero that is a feature of this ratio in all cases we have considered. The inclusion of a DqAMM shifts the zero to a larger value of x . Given the uniformly small value of this ratio and its sensitivity to the DqAMM, we judge that meson-cloud affects must play a large role on the entire domain that is currently accessible to experiment.

5 The $\gamma^* N \rightarrow R$ Roper Transition

Jefferson Lab experiments [34; 33; 35; 7] have yielded precise nucleon-Roper ($N \rightarrow R$) transition form factors and thereby exposed the first zero seen in any hadron form factor or transition amplitude. It has also attracted much theoretical attention; but Ref. [13] provides the first continuum treatment of this problem using the power of relativistic quantum field theory. That study begins with a computation of the mass and wave function of the proton and its first radial excitation. The masses are (in GeV): $M_{\text{nucleon}(N)} = 1.18$ and $M_{\text{nucleon-excited}(R)} = 1.73$. These values correspond to the locations of the two lowest-magnitude $J^P = 1/2^+$ poles in the three-quark scattering problem. The associated residues are the Faddeev wave functions, which depend upon $(p^2, p \cdot P)$, where p is the quark-diquark relative momentum. Fig. 4 depicts the zeroth Chebyshev moment of all S -wave components in that wave function. The appearance of a single zero in S -wave components of the Faddeev wave function associated with the first excited state in the three dressed-quark scattering problem indicates that this state is a radial excitation.

The empirical values of the pole locations for the first two states in the nucleon channel are [36]: 0.939 GeV and $1.36 - i0.091$ GeV, respectively. At first glance, these values appear unrelated to those obtained within the DSEs framework. However, deeper consideration reveals [37; 38] that the kernel in

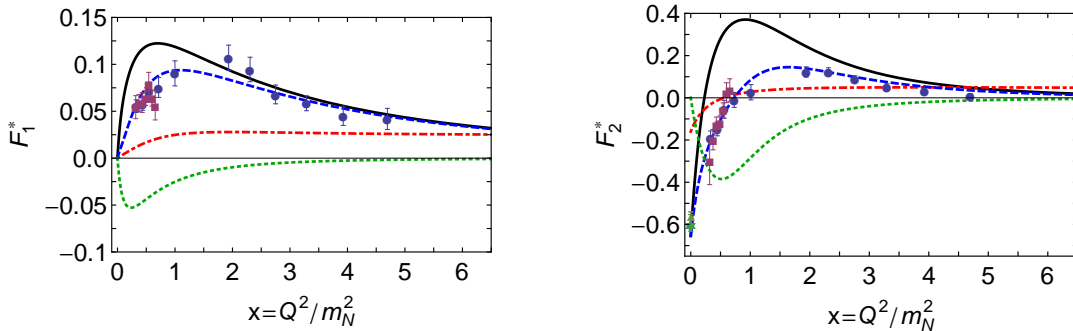


Fig. 5 *Left* – Dirac transition form factor, $F_1^*(x)$, $x = Q^2/m_N^2$. Solid (black) curve, QCD-kindred prediction; dot-dashed (red) curve, contact-interaction result; dotted (green) curve, inferred meson-cloud contribution; and dashed (blue) curve, anticipated complete result. *Right* – Pauli transition form factor, $F_2^*(x)$, with same legend. Data in both panels: circles (blue) [33]; triangle (gold) [35]; squares (purple) [7]; and star (green) [6].

the Faddeev equation omits all those resonant contributions which may be associated with the meson-baryon final-state interactions that are resummed in dynamical coupled channels models in order to transform a bare-baryon into the observed state [36; 3]. This Faddeev equation should therefore be understood as producing the dressed-quark core of the bound-state, not the completely-dressed and hence observable object. Crucial, therefore, is a comparison between the quark-core mass and the value determined for the mass of the meson-undressed bare-Roper in Ref. [36] which is 1.76 GeV.

The transition form factors are displayed in Fig. 5. The results obtained using QCD-derived propagators and vertices agree with the data on $x \gtrsim 2$. The contact-interaction result simply disagree both quantitatively and qualitatively with the data. Therefore, experiment is evidently a sensitive tool with which to chart the nature of the quark-quark interaction and hence discriminate between competing theoretical hypotheses.

The mismatch between the DSE predictions and data on $x \lesssim 2$ is due to Meson-cloud contributions that are expected to be important on this domain. An inferred form of that contribution is provided by the dotted (green) curves in Fig. 5. These curves have fallen to just 20% of their maximum value by $x = 2$ and vanish rapidly thereafter so that the DSE predictions alone remain as the explanation of the data. Importantly, the existence of a zero in F_2^* is not influenced by meson-cloud effects, although its precise location is.

6 Conclusions

We have presented a unified study of nucleon, Delta and Roper elastic and transition form factors, and compare predictions made using a framework built upon a Faddeev equation kernel and interaction vertices that possess QCD-like momentum dependence with results obtained using a symmetry-preserving treatment of a vector \otimes vector contact-interaction. The comparison emphasises that experiment is sensitive to the momentum dependence of the running coupling and masses in QCD and highlights that the key to describing hadron properties is a veracious expression of dynamical chiral symmetry breaking in the bound-state problem. Amongst our results, the following are of particular interest: The scaling behaviour of the electromagnetic ratios G_E^p/G_M^p and F_2^p/F_1^p is due to higher quark orbital angular momentum components in the nucleon wave function but also to strong diquark correlations. In fact, the presence of strong diquark correlations within the nucleon is sufficient to understand empirical extractions of the flavour-separated versions of Dirac and Pauli form factors. In connection with the $\gamma^*N \rightarrow \Delta$ transition, the momentum-dependence of the magnetic transition form factor, G_M^* , matches that of G_M^n once the momentum transfer is high enough to pierce the meson-cloud; and the electric quadrupole ratio is a keen measure of diquark and orbital angular momentum correlations, the zero in which is obscured by meson-cloud effects on the domain currently accessible to experiment. Finally, the Roper resonance is at heart of the nucleon's first radial excitation, consisting of a dressed-quark core augmented by a meson cloud that reduces its mass by approximately 20%. Our analysis shows that a meson-cloud obscures the dressed-quark core from long-wavelength probes, but that it is revealed to probes with $Q^2 \gtrsim 3m_N^2$.

Acknowledgements The material described in this contribution is drawn from work completed in collaboration with numerous excellent people, to all of whom I am greatly indebted. I would also like to thank

V. Mokeev, R. Gothe, T.-S. H. Lee and G. Eichmann for insightful comments; and to express my gratitude to the organisers of the ECT* Workshop in Trento *Nucleon Resonances: From Photoproduction to High Photon Virtualities*, whose support helped my participation. I acknowledge financial support from the Alexander von Humboldt Foundation.

References

1. I.G. Aznauryan *et al.* (2013) Studies of Nucleon Resonance Structure in Exclusive Meson Electroproduction. *Int. J. Mod. Phys. E22*: 1330015.
2. C.D. Roberts (2011) Opportunities and Challenges for Theory in the N^* program. *AIP Conf. Proc.* 1432: 19–25.
3. H. Kamano *et al.* (2013) Nucleon resonances within a dynamical coupled-channels model of πN and γN reactions. *Phys. Rev. C88*: 035209.
4. I.C. Cloët *et al.* (2013) Revealing dressed-quarks via the proton’s charge distribution. *Phys. Rev. Lett.* 111:101803.
5. L. Chang *et al.* (2013) Pion electromagnetic form factor at spacelike momenta. *Phys. Rev. Lett.* 111: 141802.
6. K.A. Olive *et al.* (Particle Data Group) (2014) The review of Particle Physics. *Chin. Phys. C38*: 090001.
7. V.I. Mokeev *et al.* (2012) Experimental Study of the $P_{11}(1440)$ and $D_{13}(1520)$ resonances from CLAS data on $ep \rightarrow e'\pi^+\pi^-p'$. *Phys. Rev. C86*: 035203.
8. V.I. Mokeev *et al.* (2013) Studies of N^* structure from the CLAS meson electroproduction data. *Int. J. Mod. Phys. Conf. Ser.* 26: 1460080.
9. J. Segovia *et al.* (2013) Insights into the $\gamma^*N \rightarrow \Delta$ transition. *Phys. Rev. C88*: 032201.
10. J. Segovia *et al.* (2013) Elastic and Transition Form Factors of the $\Delta(1232)$. *Few Body Syst* 55: 1–33.
11. J. Segovia *et al.* (2014) Nucleon and Δ elastic and transition form factors. *Few Body Syst.* 55: 1185-1222
12. J. Segovia *et al.* (2015) Understanding the nucleon as a Borromean bound-state. *Phys. Lett. B750*: 100–106.
13. J. Segovia *et al.* (2015) Completing the picture of the Roper resonance. *Phys. Rev. Lett.* 115: 171801.
14. L. Chang *et al.* (2011) Selected highlights from the study of mesons. *Chin. J. Phys.* 49: 955–1004.
15. A. Bashir *et al.* (2012) Collective perspective on advances in Dyson-Schwinger Equation QCD. *Commun. Theor. Phys.* 58: 79–134.
16. I. Cloët *et al.* (2014) Explanation and Prediction of Observables using Continuum Strong QCD. *Prog. Part. Nucl. Phys.* 77: 1–69.
17. R.T. Cahill *et al.* (1989) Baryon Structure and QCD. *Austral. J. Phys.* 42: 129–145.
18. G. Eichmann *et al.* (2010) Nucleon mass from a covariant three-quark Faddeev equation. *Phys. Rev. Lett.* 104: 201601.
19. O. Gayou *et al.* (2001) Measurements of the elastic electromagnetic form-factor ratio $\mu_p G_{Ep}/G_{Mp}$ via polarization transfer. *Phys. Rev. C64*: 038202.
20. V. Punjabi *et al.* (2005) Proton elastic form-factor ratios to $Q^2 = 3.5 \text{ GeV}^2$ by polarization transfer. *Phys. Rev. C71*: 055202.
21. A.J.R. Puckett *et al.* (2010) Recoil Polarization Measurements of the Proton Electromagnetic Form Factor Ratio to $Q^2 = 8.5 \text{ GeV}^2$. *Phys. Rev. Lett.* 104: 242301.
22. A.J.R. Puckett *et al.* (2012) Final Analysis of Proton Form Factor Ratio Data at $Q^2 = 4.0, 4.8$ and 5.6 GeV^2 . *Phys. Rev. C85*: 045203.
23. G.D. Cates *et al.* (2011) Flavor decomposition of the elastic nucleon electromagnetic form factors. *Phys. Rev. Lett.* 106: 252003.
24. H.F. Jones *et al.* (1973) Multipole $\gamma N \Delta$ form-factors and resonant photoproduction and electroproduction. *Annals Phys.* 81: 1–14.
25. G. Eichmann *et al.* (2012) Nucleon to Delta electromagnetic transition in the Dyson-Schwinger approach. *Phys. Rev. D85*: 093004.
26. M.A.B. Beg *et al.* (1964) SU(6) and electromagnetic interactions. *Phys. Rev. Lett.* 13: 514–517.
27. A.J. Buchmann (2004) Electromagnetic $N \rightarrow \Delta$ transition and neutron form-factors. *Phys. Rev. Lett.* 93: 212301.
28. Carl E. Carlson (1986) Electromagnetic $N - \Delta$ transition at high Q^2 . *Phys. Rev. D34*: 2704.
29. I. Aznauryan (2011) Results from the N^* program at JLab. *J. Phys. Conf. Ser.* 299: 012008.
30. W. Ash *et al.* (1967) Measurement of the γNN^* form factor. *Phys. Lett. B24*: 165–168.
31. B. Julia-Diaz *et al.* (2007) Extraction and Interpretation of $\gamma N \rightarrow \Delta$ Form Factors within a Dynamical Model. *Phys. Rev. C75*: 015205.
32. H. Sanchis-Alepuz *et al.* (2014) Pion cloud effects on baryon masses. *Phys. Lett. B733*: 151–157.
33. I.G. Aznauryan *et al.* (2009) Electroexcitation of nucleon resonances from CLAS data on single pion electroproduction. *Phys. Rev. C80*: 055203.
34. I.G. Aznauryan *et al.* (2012) Electroexcitation of nucleon resonances. *Prog. Part. Nucl. Phys.* 67: 1–54.
35. M. Dugger *et al.* (2009) π^+ photoproduction on the proton for photon energies from 0.725 to 2.875 GeV. *Phys. Rev. C79*: 065206.
36. N. Suzuki *et al.* (2010) Disentangling the Dynamical Origin of P_{11} Nucleon Resonances. *Phys. Rev. Lett.* 104: 042302.
37. G. Eichmann *et al.* (2008) Perspective on rainbow-ladder truncation. *Phys. Rev. C77*: 042202.
38. G. Eichmann *et al.* (2009) Toward unifying the description of meson and baryon properties. *Phys. Rev. C79*:012202.